OXFORD

SOT | Society of Toxicology
academic.oup.com/toxsci

TOXICOLOGICAL SCIENCES, 172(1), 2019, 51–62

doi: 10.1093/toxsci/kfz169
Advance Access Publication Date: July 31, 2019
Research Article

mRNA-Sequencing Identifies Liver as a Potential Target Organ for Triphenyl Phosphate in Embryonic Zebrafish

Aalekhya Reddam,[*,†] Constance A. Mitchell,[*,†] Subham Dasgupta,[†] Jay S. Kirkwood,[‡] Alyssa Vollaro,[‡] Manhoi Hur,[‡] and David C. Volz[†,1]

[*]Environmental Toxicology Graduate Program; [†]Department of Environmental Sciences; and [‡]Metabolomics Core Facility, Institute for Integrative Genome Biology, University of California, Riverside, California 92521

[1]To whom correspondence should be addressed at Department of Environmental Sciences, University of California, Riverside, CA 92521. Fax: (951) 827-4652. E-mail: david.volz@ucr.edu.

ABSTRACT

Triphenyl phosphate (TPHP) is a commonly used organophosphate flame retardant and plasticizer in the United States. Using zebrafish as a model, the overall objective of this study was to identify potential organs that might be targeted by TPHP during embryonic development. Based on mRNA-sequencing, TPHP exposure from 24 to 30 h post fertilization (hpf) and 24 to 48 hpf significantly affected the abundance of 305 and 274 transcripts, respectively, relative to vehicle (0.1% DMSO) controls. In addition to minor effects on cardiotoxicity- and nephrotoxicity-related pathways, ingenuity pathway analysis (IPA) of significantly affected transcripts within 30- and 48-hpf embryos revealed that hepatotoxicity-related pathways were strongly affected following exposure to TPHP-alone. Moreover, although pretreatment with fenretinide (a retinoic acid receptor agonist) mitigated TPHP-induced pericardial edema and liver enlargement at 72 and 128 hpf, respectively, IPA revealed that fenretinide was unable to block TPHP-induced effects on cardiotoxicity-, nephrotoxicity-, and hepatotoxicity-related pathways at 48 hpf, suggesting that TPHP-induced effects on the transcriptome were not associated with toxicity later in development. In addition, based on Oil Red O staining, we found that exposure to TPHP nearly abolished neutral lipids from the embryonic head and trunk and, based on metabolomics, significantly decreased the total abundance of metabolites—including betaine, a known osmoprotectant—at 48 and 72 hpf. Overall, our data suggest that, in addition to the heart, TPHP exposure during early development results in adverse effects on the liver, lipid utilization, and osmoregulation within embryonic zebrafish.

Key words: triphenyl phosphate; heart; liver; betaine; osmoregulation; zebrafish.

Triphenyl phosphate (TPHP) is an unsubstituted aryl phosphate ester that is widely used as an additive flame retardant and plasticizer (van der Veen and de Boer, 2012). Within the built environment, TPHP migrates out of end-use products via leaching and volatilization, resulting in accumulation within indoor dust (Stapleton *et al.*, 2009). As such, TPHP is ubiquitous within indoor dust samples around the world, where concentrations ranging from 0.24 to 1 789 000 ng/g have been detected within indoor dust samples in the United States, Australia, Egypt, Canada, Germany, Finland, Kazakhstan, United Kingdom, and China (Harrad *et al.*, 2016; Khairy and Lohmann, 2019; Rantakokko *et al.*, 2019; Stapleton *et al.*, 2009; Sun *et al.*, 2019). Due to the presence of TPHP within indoor dust, humans are exposed to TPHP through ingestion, inhalation, and dermal absorption, resulting in frequent detection of the primary metabolite of TPHP—diphenyl phosphate (DPHP)—in urine, blood serum, breast milk, and placental tissue (Ding *et al.*, 2016; He *et al.*, 2018; Kim *et al.*, 2014; Ospina *et al.*, 2018; Sun *et al.*, 2018).

Prior studies conducted *in vitro* have shown that TPHP induces cytotoxicity in chicken embryonic hepatocytes (Su *et al.*, 2014), and induces intracellular reactive oxygen species

generation, apoptosis, and cell cycle arrest in HepG2 cells (An *et al.*, 2018). Within invertebrates, TPHP disrupts the metabolome in both earthworms and freshwater algae, leading to downstream effects on membrane integrity (Wang *et al.*, 2018, 2019b). TPHP also disrupts lipid metabolism through inhibition of carboxylesterase, resulting in an increase in body weight, liver weight, and hepatic steatosis in male mice (Morris *et al.*, 2014; Wang *et al.*, 2019a). In aquatic vertebrates, TPHP induces neurotoxicity in Chinese rare minnows and reproductive toxicity in Japanese medaka (Hong *et al.*, 2018; Li *et al.*, 2018), and, in zebrafish, induces thyroid endocrine disruption, developmental neurotoxicity, ocular toxicity, and hepatotoxicity (Du *et al.*, 2016; Jarema *et al.*, 2015; Kim *et al.*, 2015; Liu *et al.*, 2016; Shi *et al.*, 2018, 2019).

Our prior studies have shown that exposure of developing zebrafish embryos to TPHP reliably induces cardiotoxicity and pericardial edema in a concentration-dependent manner (Isales *et al.*, 2015; McGee *et al.*, 2013; Mitchell *et al.*, 2018). Although TPHP-induced cardiotoxicity is independent of the aryl hydrocarbon receptor (McGee *et al.*, 2013), TPHP-cardiotoxicity is enhanced in the presence of nontoxic concentrations of a pan-retinoic acid receptor (RAR) antagonist (BMS493) (Isales *et al.*, 2015) and mitigated by pretreatment with nontoxic concentrations of a pan-RAR agonist (fenretinide) (Mitchell *et al.*, 2018), suggesting that RAR may be involved in mediating the effects of TPHP within developing zebrafish embryos. Retinoic acid signaling regulates development and differentiation of many tissues, organs, and processes within zebrafish, including but not limited to hindbrain patterning, heart morphogenesis, lipid abundance, and kidney/liver development (Begemann *et al.*, 2004; Samarut *et al.*, 2015; Stafford and Prince, 2002; Stainier and Fishman, 1992; Wingert *et al.*, 2007; Yutzey and Bader, 1995). Therefore, in addition to the heart, RAR-mediated TPHP toxicity may be impacting other organs in the zebrafish embryo.

Using zebrafish as a model, the overall objective of this study was to identify other potential organs that might be targeted by TPHP during embryonic development. To accomplish this objective, we relied on whole-embryo exposures and a combination of mRNA-sequencing, phenotypic assessments, neutral lipid staining, and metabolomics to test the hypothesis that TPHP interferes with normal development of other organ systems—effects that, similar to our findings with the heart, may be mitigated by pretreatment with an RAR agonist (fenretinide).

MATERIALS AND METHODS

Animals. Adult wildtype (5D) zebrafish were maintained and bred on a recirculating system using previously described procedures (Mitchell *et al.*, 2018). Adult breeders were handled and treated in accordance with Institutional Animal Care and Use Committee-approved animal use protocol (No. 20150035 and No. 20180063) at the University of California, Riverside.

Chemicals. TPHP (99.5% purity) was purchased from ChemService, Inc (West Chester, Pennsylvania), whereas fenretinide (> 99.3% purity) was purchased from Tocris Bioscience (Bristol, United Kingdom). All stock solutions were prepared by dissolving chemicals in high performance liquid chromatography-grade dimethyl sulfoxide (DMSO). TPHP and fenretinide were stored at room temperature and 4°C, respectively, in 2-ml amber glass vials with polytetrafluoroethylene-lined caps. Working solutions were freshly prepared by spiking stock solutions into particulate-free water from our recirculating system (pH and conductivity of approximately 7.2 and 950 μS, respectively), resulting in 0.1% DMSO within all vehicle control and treatment groups. Tricaine methanesulfonate (MS-222) (Western Chemical, Inc, Ferndale, Washington) solutions were freshly made by dissolving MS-222 into particulate-free water from our recirculating system. Propylene glycol (> 99.5% purity) and Oil Red O (> 75% dye content) were purchased from Fisher Scientific (Hampton, New Hampshire) and Sigma-Aldrich (St Louis, Missouri), respectively.

Phenotypic assessments. Newly fertilized eggs were collected immediately following spawning and incubated in groups of approximately 100 per 100 × 15 mm polystyrene petri dish within a light- and temperature-controlled incubator until 24 h post fertilization (hpf). Viable embryos were transferred to 100 × 15 mm polystyrene petri dishes containing 10 ml of either vehicle (0.1% DMSO) or 10 μM TPHP, resulting in 30 initial embryos per dish (3 dishes per treatment). All dishes were then covered with a plastic lid and incubated under static conditions at 28°C under a 14:10-h light-dark cycle until either 30, 48, or 72 hpf. Supplementary Figure 1 provides an overview of exposure scenarios used for all experiments throughout this study.

At 30, 48, or 72 hpf, embryos were removed from the incubator and anesthetized with 100 mg/l MS-222 by adding 5 ml of 300 mg/l MS-222 to each petri dish; 30-hpf embryos were dechorionated by incubating in 0.3 mg/ml pronase for 10 min. Surviving embryos (≥ 80% survival across all treatment groups) were then transferred to black 384-well microplates with 0.17-mm glass-bottom wells (Matrical Bioscience, Spokane, Washington), and each plate was centrifuged at 200 rpm for 3 min to orient hatched embryos in right or left lateral recumbency. Embryos were then imaged under transmitted light using automated image acquisition protocols and parameters previously optimized for our ImageXpress Micro XLS Widefield High-Content Screening System (Molecular Devices, Sunnyvale, California) (Yozzo *et al.*, 2013). Following image acquisition, embryos were then euthanized by placing the plate at 4°C for 30 min. Body length (μm) and pericardial area (μm^2) were quantified within MetaXpress 6.0.3.1658 (Molecular Devices) using previously described protocols (Yozzo *et al.*, 2013).

To identify potential effects of TPHP on liver morphology, embryos (30 per dish; 3 dishes per treatment) were exposed to either vehicle (0.1% DMSO) or 5 μM TPHP from 30 to 72 hpf as described above, and then transferred to system water from 72 to 128 hpf (Supplementary Figure 1). As exposure to 10 μM TPHP from 30 to 72 hpf resulted in significant mortality at 128 hpf (< 50% survival), we relied on 5 μM TPHP as the maximum tolerated concentration in the absence of significant mortality (≥ 80% survival) for liver morphology assessments. At 128 hpf, all embryos were fixed overnight in 4% paraformaldehyde, transferred to 1× phosphate buffer solution (PBS), oriented in right lateral recumbency, and imaged under transmitted light at ×3.2 magnification using a Leica MZ10 F stereomicroscope equipped with a DMC2900 camera. Liver area (μm^2) was then quantified within ImageJ.

Fenretinide pretreatments. Embryos were pretreated with 10 ml of vehicle (0.1% DMSO) or 2 μM fenretinide from 24 to 30 hpf as described above, and then transferred to clean petri dishes and exposed to 10 ml of vehicle (0.1% DMSO) or 10 μM TPHP from 30 to 48 hpf or 30 to 72 hpf as described above (Supplementary Figure 1). Procedures for phenotypic assessments were identical to those described above.

mRNA-sequencing. To assess the potential effects of TPHP on the embryonic transcriptome at 30 and 48 hpf (experiment no. 1),

24-hpf embryos (30 embryos per petri dish; 6 petri dishes per treatment) were exposed to 10 ml of vehicle (0.1% DMSO) or 10 μM TPHP as described above (Supplementary Figure 1). At 30 and 48 hpf, 2 petri dishes containing up to 30 embryos each were pooled into one 2-ml cryovial and snap-frozen in liquid nitrogen, resulting in up to 60 embryos per vial and 3 replicate 2-ml cryovials per treatment per time-point. To determine whether fenretinide pretreatment mitigated TPHP-induced effects on the embryonic transcriptome at 48 hpf (experiment no. 2), 24-hpf embryos (30 embryos per petri dish; 6 petri dishes per treatment) were pretreated with 10 ml of vehicle (0.1% DMSO) or 2 μM fenretinide from 24 to 30 hpf, and then transferred to clean petri dishes and exposed to 10 ml of vehicle (0.1% DMSO) or 10 μM TPHP from 30 to 48 hpf as described above. At 48 hpf, 2 petri dishes containing up to 30 embryos each were pooled into one 2-ml cryovial and snap-frozen in liquid nitrogen, resulting in up to 60 embryos per vial and 3 replicate 2-ml cryovials per treatment per time-point. All samples (24 total) were stored at −80°C until total RNA extraction.

Embryos were homogenized in 2-ml cryovials using a PowerGen Homogenizer (ThermoFisher Scientific, Waltham, Massachusetts), resulting in a total of 24 samples. Following homogenization, an SV Total RNA Isolation System (Promega, Madison, Wisconsin) was used to extract total RNA from each replicate sample following the manufacturer's instructions. RNA quantity and quality were confirmed using a Qubit 4.0 Fluorometer (ThermoFisher Scientific) and 2100 Bioanalyzer system (Agilent, Santa Clara, California), respectively. Based on sample-specific Bioanalyzer traces, the RNA Integrity Number (RIN) was >8 for all RNA samples used for library preparations. Libraries were prepared using a QuantSeq 3′ mRNA-Seq Library Prep Kit FWD (Lexogen, Vienna, Austria) and indexed by treatment replicate following the manufacturer's instructions. Library quality and quantity were confirmed using a Qubit 4.0 Fluorometer and 2100 Bioanalyzer system, respectively. Libraries were then pooled by experiment number, diluted to a concentration of 1.3 pM (with 1% PhiX control), and single-read (1X75) sequenced on our Illumina MiniSeq Sequencing System (San Diego, California) using 3 separate 75-cycle High-Output Reagent Kits (2 replicate kits for experiment no. 1; 1 kit for experiment no. 2).

All sequencing data were uploaded to Illumina's BaseSpace in real-time for downstream analysis of quality control. Raw Illumina (fastq.gz) sequencing files (36 files) are available via NCBI's BioProject database under BioProject ID PRJNA529921, and a summary of sequencing run metrics are provided in Supplementary Tables 1, 4, and 11 ($>83\%$ of reads were $\geq$Q30 across all runs). All 36 raw and indexed Illumina (fastq.gz) sequencing files were downloaded from BaseSpace and uploaded to Bluebee's genomics analysis platform to align reads against zebrafish genome assembly GRCz10. After combining treatment replicate files, a DESeq2 application within Bluebee (Lexogen Quantseq DE 1.2) was used to identify significant treatment-related effects on transcript abundance (relative to vehicle controls) based on a false discovery rate (FDR) p-adjusted value $<.01$. Using DESeq2-identified transcripts with a FDR p-adjusted value $<.01$, downstream analyses were run using Qiagen's ingenuity pathway analysis (IPA) (Germantown, Maryland). Statistically significant transcripts were uploaded to IPA, and human, rat, and mouse homologs were automatically identified within IPA using NCBI's HomoloGene. A Tox Analysis was then performed using a Fisher's Exact Test p-value threshold of .05 as the basis for identifying statistically significant pathways; the algorithm considered both direct and indirect relationships using Ingenuity Knowledge Base (genes only) as the reference set. In addition, for experiment no. 2, significantly affected transcripts were imported into the Database for Annotation, Visualization and Integrated Discovery (DAVID) v6.8 for Gene Ontology (GO) enrichment analysis, using a count of 2 and an EASE of 1.

Oil Red O staining. Embryos were exposed to either vehicle (0.1% DMSO) or TPHP (2.5, 5, or 10 μM) from 24 to 72 hpf as described above. In addition, embryos were pretreated with 2 μM fenretinide and then exposed to 10 μM TPHP as described above (Supplementary Figure 1). At 72 hpf, embryos were fixed in 4% paraformaldehyde for 24 h and then transferred to 1× PBS. Fixed embryos were stained with Oil Red O using previously described protocols (Passeri *et al.*, 2009). Briefly, whole fixed embryos were infiltrated with a graded series of propylene glycol and then stained with 0.5% Oil Red O in 100% propylene glycol overnight. Stained embryos were washed with decreasing concentrations of propylene glycol, rinsed several times with 1× PBS, and then stored in 1× PBS at 4°C. Stained embryos were imaged using under transmitted light at ×4 magnification using a Leica MZ10 F stereomicroscope equipped with a DMC2900 camera. Mean color intensity within stained embryos was quantified using the mean gray value within ImageJ.

Untargeted metabolomics. Embryos (30 embryos per petri dish; 3 petri dishes per treatment) were exposed to 10 ml of vehicle (0.1% DMSO) or 10 μM TPHP from 24 to 48 hpf or 24 to 72 hpf as described above (Supplementary Figure 1). At 48 and 72 hpf, embryos from replicate dishes were transferred to 1.5-ml microcentrifuge tubes, snap-frozen in liquid nitrogen, and stored at −80°C until extractions. For all extractions, 500 μl of ice-cold solvent (30:30:20:20 MeOH:ACN:IPA:water) was added to each tube, and tubes were then sonicated for 15 min, vortexed for 15 min, sonicated for 15 min, and centrifuged at 16 000 × g at 4°C for 15 min. The supernatant was then transferred to glass HPLC vials for LC-MS analysis.

LC-MS was performed on a Synapt G2-Si quadrupole time-of-flight mass spectrometer (Waters, Milford, Massachusetts) coupled to a I-class UPLC system (Waters). Separations were carried out on a CSH C18 column (2.1 × 100 mm, 1.7 μM) (Waters). The mobile phases were (A) 60:40 acetonitrile:water with 10 mM ammonium formate and 0.1% formic acid, and (B) 90:10 isopropanol:acetonitrile with 10 mM ammonium formate and 0.1% formic acid. The flow rate was 350 μl/min and the column was held at 50°C. The injection volume was 4 μl. The following gradient program (with respect to mobile phase B) was used: 0 min, 10% B; 1 min, 10% B; 3 min, 20% B; 5 min, 40% B; 16 min, 80% B; 18 min, 99% B; 20 min 99% B; 20.5 min, 10% B. Prior to LC-MS analysis, samples were diluted 20-fold to prevent detector saturation. The MS was operated in positive ion mode (50–1200 m/z) with a 100-ms scan time. Source and desolvation temperatures were 120°C and 500°C, respectively. Desolvation and cone gas were set to 1000 and 150 l/h, respectively. All gases were (generated by pooling equal aliquots of each sample) was analyzed every 4–5 injections to monitor system stability and performance. Samples were analyzed in random order. Leucine enkephalin was infused and used for mass correction.

Untargeted data processing (peak picking, alignment, deconvolution, integration, normalization, and spectral matching) was performed in Progenesis Qi software (Nonlinear Dynamics, Durham, North Carolina). Data were normalized to total ion abundance. Features with a CV greater than 20% or with an average abundance less than 200 in the quality control injections

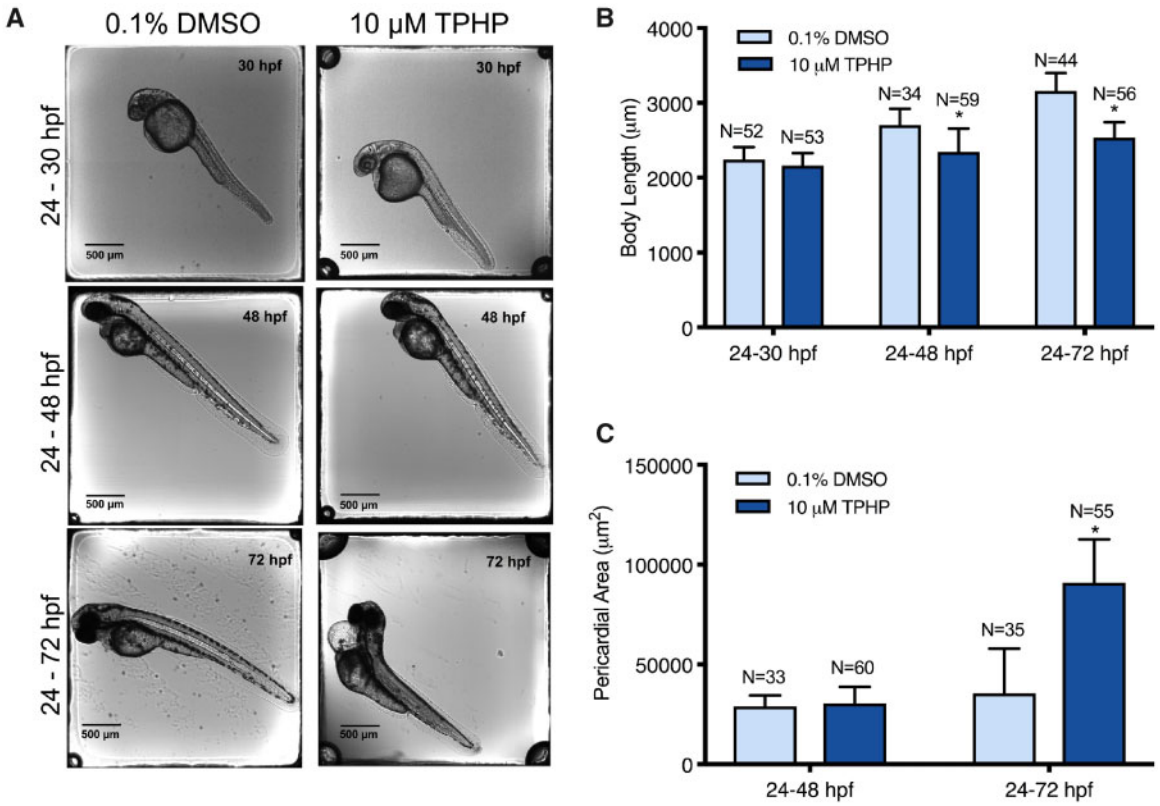

Figure 1. Representative images (A), mean body length (± standard deviation) (B), and mean pericardial area (± standard deviation) (C) of 30-, 48-, and 72-hpf embryos treated with either vehicle (0.1% DMSO) or 10 μM TPHP (triphenyl phosphate) from 24 to 30 hpf, 24 to 48 hpf, or 24 to 72 hpf. Asterisk (*) denotes $p < .05$.

were removed (Dunn *et al.*, 2011). To help identify features that belong to a single metabolite, features were assigned a cluster ID using RAMClust (Broeckling *et al.*, 2014). An extension of the metabolomics standard initiative guidelines was used to assign annotation level confidence (Schymanski *et al.*, 2014; Sumner *et al.*, 2007). Several MS/MS metabolite databases were searched against including Metlin, Mass Bank of North America, Lipidblast, and an in-house database.

Liver histology. To identify potential effects of TPHP on hepatic tissue with or without fenretinide pretreatment, embryos were (1) pretreated with 10 ml of vehicle (0.1% DMSO) or 2 μM fenretinide from 24 to 30 hpf as described above; (2) transferred to clean petri dishes and exposed to 10 ml of vehicle (0.1% DMSO) or 5 μM TPHP from 30 to 72 hpf and; (3) transferred to system water from 72 to 128 hpf (Supplementary Figure 1). At 128 hpf, embryos were fixed overnight in 4% paraformaldehyde, transferred to 1× PBS, and immediately shipped to HistoWiz Inc (Brooklyn, New York) for histology procedures. Samples were then oriented in right lateral recumbency, paraffin-embedded, and 4-μm thick-step sections through the whole body were mounted on glass slides and stained with hematoxylin and eosin (H&E). After staining, sections were dehydrated and film cover-slipped using a Tissue-Tek Prisma and Coverslipper (Sakura Finetek USA, Inc, Torrance, California). Whole-slide scanning was performed on an Aperio AT2 (Leica Biosystems, Wetzlar, Germany) using a 40× objective, and digital slides were transferred from HistoWiz to our lab for qualitative assessments.

Statistical analyses. For all phenotypic data, a general linear model (GLM) analysis of variance (ANOVA) ($\alpha = .05$) was performed using SPSS Statistics 24, as these data did not meet the equal variance assumption for non-GLM ANOVAs. Treatment groups were compared with vehicle controls using pairwise Tukey-based multiple comparisons of least square means to identify significant differences. For metabolomics data, Q values were generated by performing the Benjamini-Hochberg correction of *p*-values generated from an ANOVA in R using the aov function. Z-scores were calculated by subtracting mean relative abundance values for each treatment group from individual replicate relative abundance values, and then dividing this number by the standard deviation for each treatment group.

RESULTS

mRNA-sequencing Reveals That TPHP Exposure Affects Transcripts Associated With Cardiotoxicity-, Hepatotoxicity-, and Nephrotoxicity-related Pathways

Our previous studies demonstrated that exposure to 5, 10, and 20 μM TPHP from 24 to 72 hpf reliably induced pericardial edema in zebrafish embryos (Mitchell *et al.*, 2018). Therefore, we selected 10 μM TPHP as an optimal concentration for the majority of exposures and pretreatment experiments. Relative to vehicle controls, initiation of exposure to 10 μM TPHP at 24 hpf resulted in (1) a significant decrease in body length at 48 and 72 hpf (but not 30 hpf) (Figs. 1A and 1B) and (2) a significant increase in pericardial area at 72 hpf (but not 48 hpf) (Figs. 1A and 1C).

Individual raw DESeq2 outputs following exposure to 10 μM TPHP from 24 to 30 hpf and 24 to 48 hpf are provided within Supplementary Tables 2, 3, 5, and 6 for sequencing replicates nos. 1 and 2, respectively. Combined raw DESeq2 outputs for exposures from 24 to 30 hpf and 24 to 48 hpf are provided within

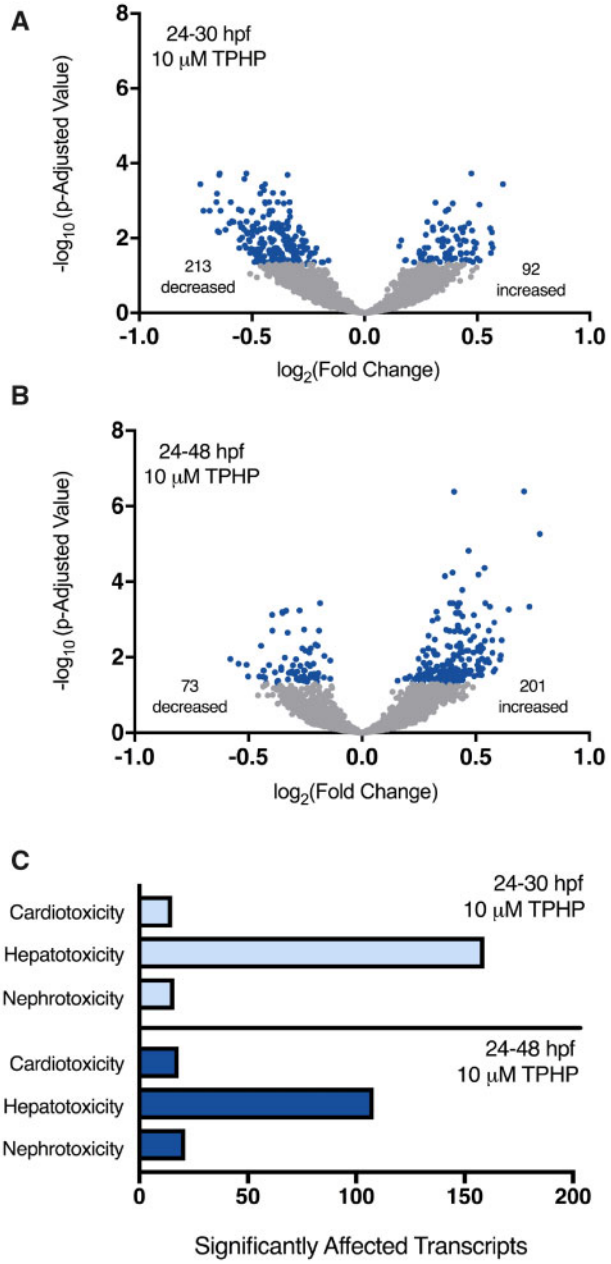

Figure 2. Volcano plots showing the number of significantly different transcripts (dark circles) following treatment with 10 μM TPHP (triphenyl phosphate) from 24 to 30 hpf (A) or 24 to 48 hpf (B) relative to vehicle (0.1% DMSO) controls. Log_2-transformed fold change is plotted on the x-axis and log_{10}-transformed *p*-adjusted value is plotted on the y-axis. Transcripts associated with cardiotoxicity-, hepatotoxicity-, and nephrotoxicity-related pathways were identified by ingenuity pathway analysis's (IPA's) toxicity analysis using a Fisher's Exact *p*-value of ≤ .05 (C).

Supplementary Tables 7 and 8, respectively. Following exposure from 24 to 30 hpf, TPHP exposure resulted in a significant decrease and increase in the abundance of 213 and 92 transcripts (305 total), respectively, at 30 hpf (Figure 2A). Following exposure from 24 to 48 hpf, TPHP exposure resulted in a significant decrease and increase in the abundance of 73 and 201 transcripts (274 total), respectively, at 48 hpf (Figure 2B).

Statistically significant transcripts with human, rat, or mouse homologs were included within IPA's Tox Analysis. Approximately 50% of statistically significant transcripts were

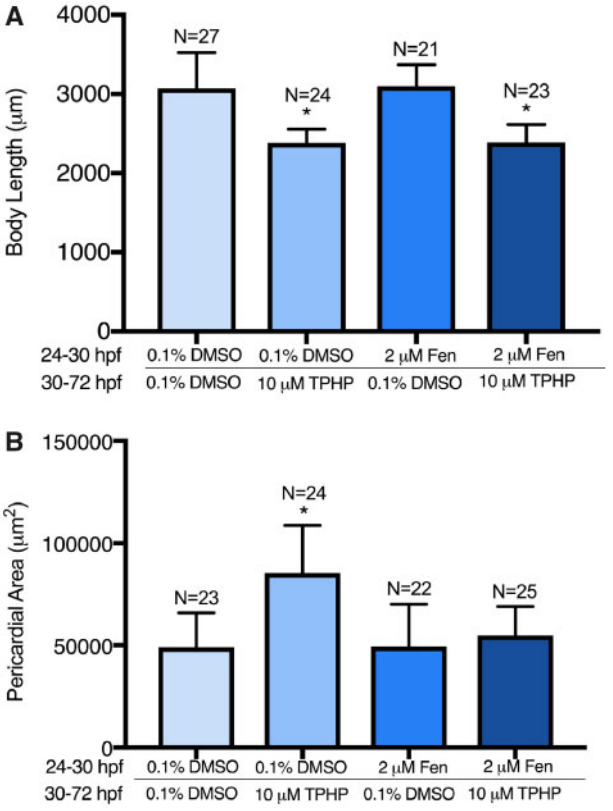

Figure 3. Mean body length (± standard deviation) (A) and mean pericardial area (± standard deviation) (B) of embryos pretreated with either vehicle (0.1% DMSO) or 2 μM fenretinide (Fen) from 24 to 30 hpf and then treated with vehicle (0.1% DMSO) or 10 μM TPHP (triphenyl phosphate) from 30 to 48 hpf (A) or 30 to 72 hpf (A, B). Asterisk (*) denotes $p < .05$.

included in IPA's Tox Analysis; the remaining statistically significant transcripts were excluded by IPA's Tox Analysis due to the absence of human, rat, and/or mouse orthologs within NCBI's Homologene database. A list of significantly affected pathways identified by IPA's Tox Analysis for 24–30 hpf and 24–48 hpf are provided within Supplementary Tables 9 and 10, respectively. Based on this analysis, pathways associated with cardiotoxicity-, hepatotoxicity-, and nephrotoxicity-related pathways were significantly affected, where the abundance of transcripts associated with hepatotoxicity was > 5-fold higher than the abundance of transcripts associated with cardiotoxicity and nephrotoxicity pathways (Figure 2C).

Pretreatment With Fenretinide Does Not Mitigate TPHP-induced Effects on Cardiotoxicity-, Hepatotoxicity-, and Nephrotoxicity-related Pathways

Our previous studies demonstrated that pretreatment with 2 μM fenretinide reliably blocked pericardial edema (but not body length) following exposure to 20 μM TPHP (Mitchell *et al.*, 2018). Likewise, within this study pretreatment with 2 μM fenretinide from 24 to 30 hpf significantly mitigated TPHP-induced pericardial edema (but not effects on body length) following exposure to 10 μM TPHP from 30 to 72 hpf (Figs. 3A and 3B).

Raw DESeq2 output is provided within Supplementary Tables 12–14. Based on these data, TPHP exposure from 30 to 48 hpf resulted in a significant effect on the abundance of 150 transcripts (14 decreased and 136 increased) at 48 hpf relative to vehicle controls (Figure 4A). Although pretreatment with

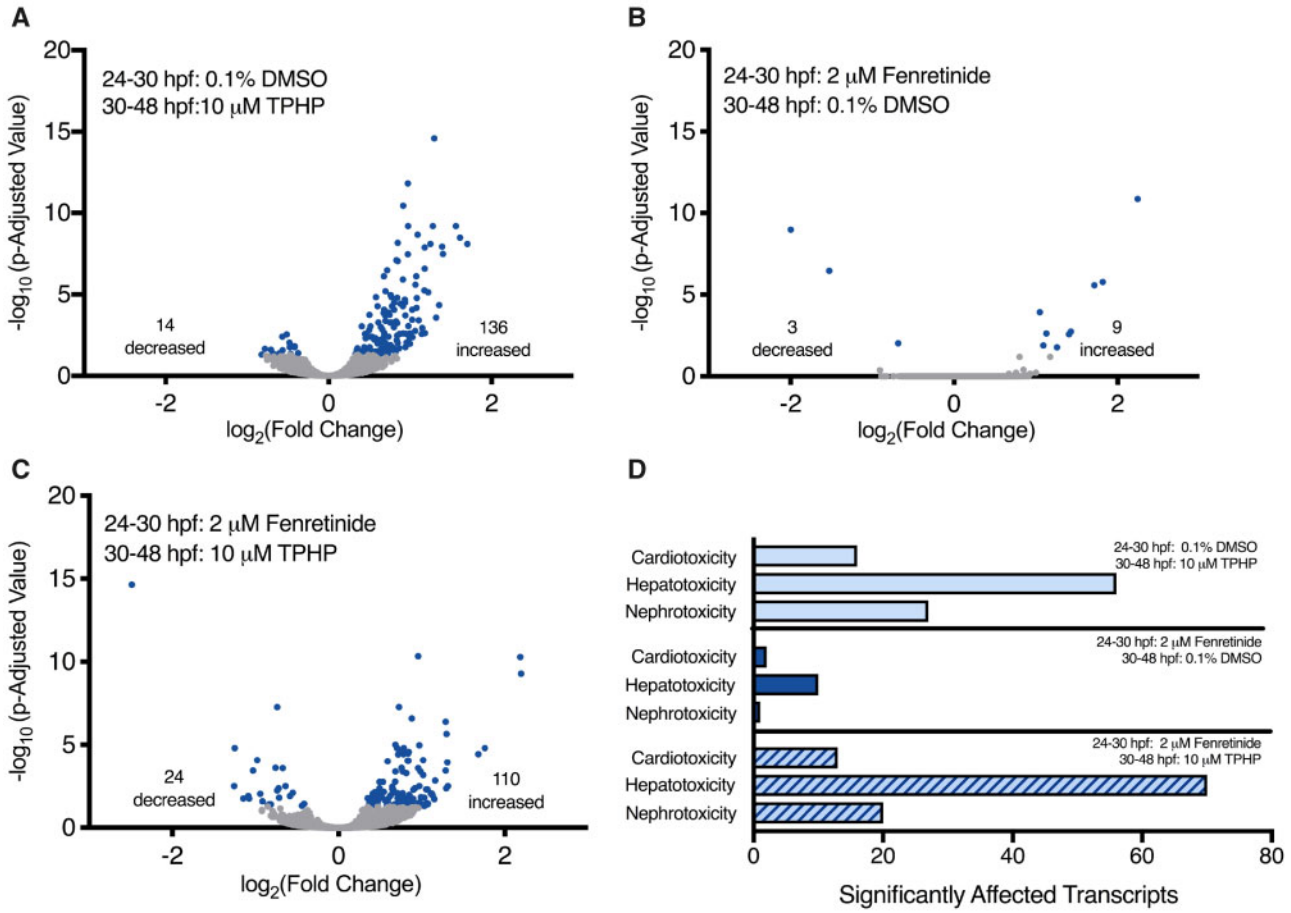

Figure 4. Volcano plots (A, B, and C) showing the number of significantly different transcripts (dark circles) at 48 hpf following pretreatment with vehicle (0.1% DMSO) or 2 μM fenretinide from 24 to 30 hpf followed by treatment with vehicle (0.1% DMSO) or 10 μM TPHP (triphenyl phosphate) from 30 to 48 hpf; all 3 plots are relative to treatment with vehicle (0.1% DMSO) from 24 to 48 hpf. Log_2-transformed fold change is plotted on the x-axis and log_{10}-transformed *p*-adjusted value is plotted on the y-axis. Transcripts associated with cardiotoxicity-, hepatotoxicity-, and nephrotoxicity-related pathways were identified by ingenuity pathway analysis's (IPA's) toxicity analysis using a Fisher's Exact *p*-value of $\leq .05$ (D).

fenretinide from 24 to 30 hpf only affected 12 transcripts (3 decreased and 9 increased) at 48 hpf (Figure 4B), pretreatment with fenretinide from 24 to 30 hpf followed by TPHP exposure from 30 to 48 hpf significantly affected the abundance of 134 transcripts (24 decreased and 110 increased) at 48 hpf (Figure 4C).

Statistically significant transcripts were included in DAVID's Biological Process analysis, and available human, rat, or mouse homologs were included in IPA's Tox Analysis. A list of significantly affected biological processes identified by DAVID for all 3 treatment groups (relative to vehicle controls) are provided within Supplementary Tables 15–17. Although pretreatment with fenretinide from 24 to 30 hpf did not alter the majority of TPHP-induced biological processes identified by DAVID (Supplementary Figure 2), fenretinide blocked TPHP-induced effects on regulation of cell cycle and ion transport.

Similar to experiment no. 1, approximately 50% of statistically significant transcripts were included in IPA's Tox Analysis; the remaining statistically significant transcripts were excluded by IPA's Tox Analysis due to the absence of human, rat, and/or mouse orthologs within NCBI's Homologene database. A list of significantly affected pathways identified by IPA's Tox Analysis for all 3 treatment groups (relative to vehicle controls) are provided within Supplementary Tables 18–20. Similar to embryos treated with TPHP-alone from 24 to 30 hpf and 24 to 48 hpf (Figure 2C), cardiotoxicity-, hepatotoxicity-, and nephrotoxicity-related pathways were significantly affected in all 3 treatment groups (Figure 4D). Interestingly, although fenretinide mitigated TPHP-induced pericardial edema (Figure 2C), fenretinide did not mitigate the effect of TPHP on cardiotoxicity-, hepatotoxicity-, and nephrotoxicity-related pathways (Figure 4D).

TPHP Induces Liver Enlargement in the Absence of Hepatocellular Toxicity

Exposure to 5 μM TPHP from 30 to 72 hpf resulted in a significant decrease in body length at 128 hpf relative to vehicle controls (Figure 5B). This effect was not mitigated by pretreatment with 2 μM fenretinide, as pretreatment with 2 μM fenretinide from 24 to 30 hpf followed by exposure to vehicle (0.1% DMSO) from 30 to 72 hpf also resulted in a significant decrease in body length at 128 hpf (Figure 5B). In addition, exposure to 5 μM TPHP from 30 to 72 hpf resulted in an increase in liver area in 128-hpf embryos relative to vehicle controls (Figs. 5A and 5C)—an effect that was mitigated by pretreatment with 2 μM fenretinide from 24 to 30 hpf. When liver area was normalized to body length, exposure to 5 μM TPHP resulted in a significantly higher liver area to body length ratio, an effect that was also mitigated by pretreatment with 2 μM fenretinide (Figure 5D). Interestingly, although liver area at 128 hpf was increased following exposure to

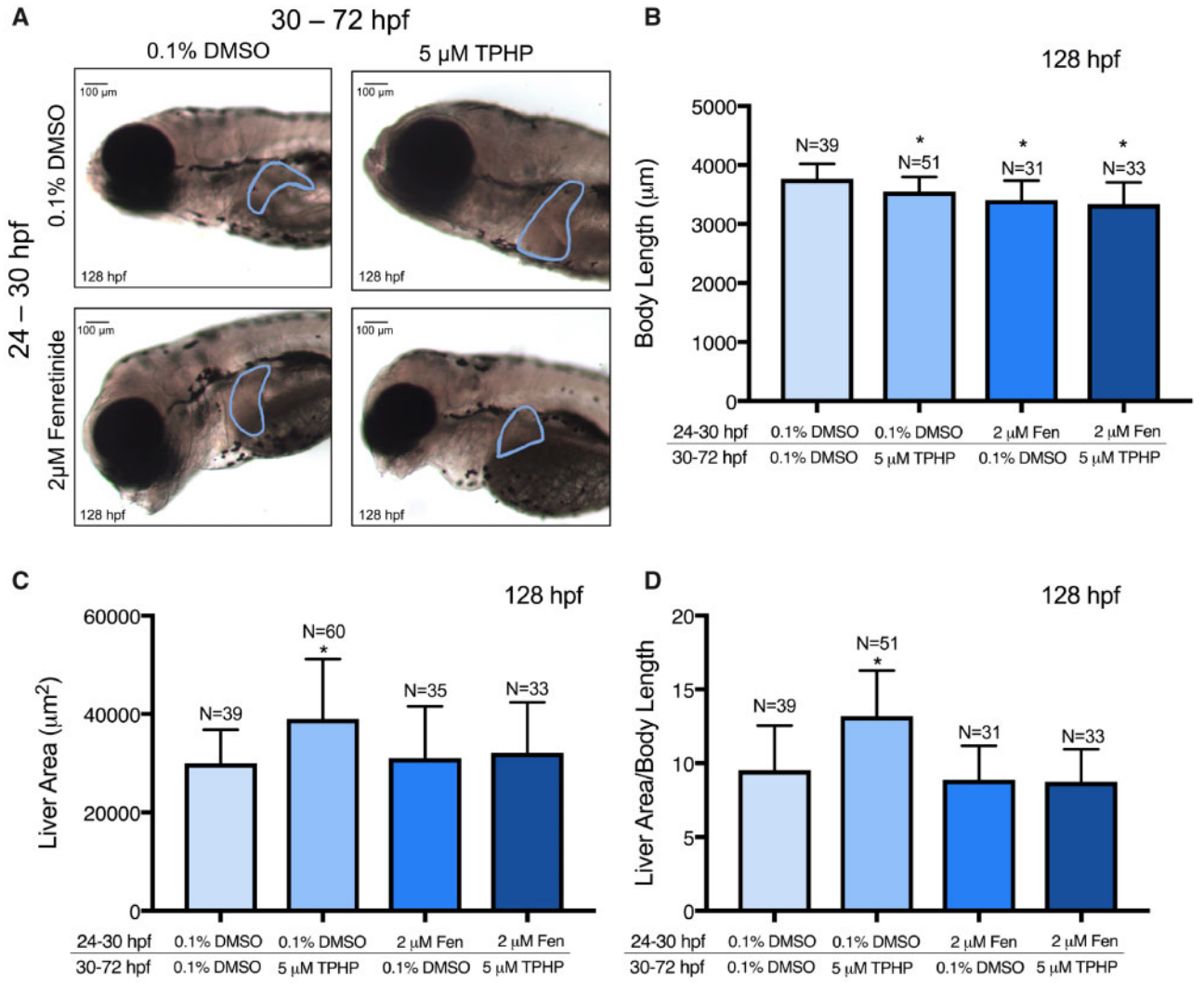

Figure 5. Representative brightfield images (A), mean body length (± standard deviation) (B), mean liver area (± standard deviation) (C), and mean body length-normalized liver area (± standard deviation) (D) of 128-hpf embryos pretreated with either vehicle (0.1% DMSO) or 2 μM fenretinide (Fen) from 24 to 30 hpf, treated with vehicle (0.1% DMSO) or 5 μM TPHP (triphenyl phosphate) from 30 to 72 hpf, and then reared in clean system water until 128 hpf. Within Panel A, the border denotes an outline of the liver on the left lateral side of a 128-hpf embryo. Asterisk (*) denotes $p < .05$.

TPHP, H&E-stained histologic sections from TPHP-exposed livers were qualitatively similar to livers from vehicle controls and embryos pretreated with 2 μM fenretinide followed by exposure to vehicle or TPHP (Figure 6). Overall, these data suggest that, at 128 hpf, TPHP exposure from 30 to 72 hpf resulted in liver enlargement in the absence of hepatocellular toxicity (based on histology), an effect that, similar to pericardial edema, was mitigated by pretreatment with fenretinide.

TPHP Induces Significant Changes in Embryonic Lipids and Metabolites

Neutral lipid abundance within the whole embryo was measured using Oil Red O staining; representative images are provided in Figure 7A. Exposure to 2.5, 5, and 10 μM of TPHP from 24 to 72 hpf resulted in a concentration-dependent decrease in the color intensity of Oil Red O within the total body (Supplementary Figure 3), pericardial region (Supplementary Figure 3), yolk sac (Supplementary Figure 3), head (Figure 7B), and trunk (Figure 7C). Interestingly, exposure to 10 μM TPHP from 30 to 72 hpf affected biological processes associated with tricarboxylic acid cycle and sphingolipid metabolic process (Supplementary Figure 2), an effect that was driven by 4 transcripts (*cs*, *sdhc*, *serinc1*, and *psap*) (Supplementary Table 12). However, pretreatment with 2 μM fenretinide from 24 to 30 hpf did not block TPHP-induced effects on Oil Red O-specific color intensity within the embryonic head and trunk (Figs. 7D and 7E).

All metabolites quantified using untargeted metabolomics are provided within Supplementary Table 21. Despite strong stage-dependent differences in metabolite abundances between 48 and 72 hpf (Figure 8A), the total abundance of all metabolites was significantly decreased following exposure to 10 μM TPHP from 30 to 48 hpf and 30 to 72 hpf (Figure 8B). Out of 102 metabolites that were identified, betaine was the most significantly affected metabolite at 48 and 72 hpf following exposure to vehicle (0.1% DMSO) or 10 μM TPHP (Figure 8C).

DISCUSSION

Although TPHP is known to disrupt cardiac looping and induce pericardial edema in zebrafish embryos (Isales *et al.*, 2015;

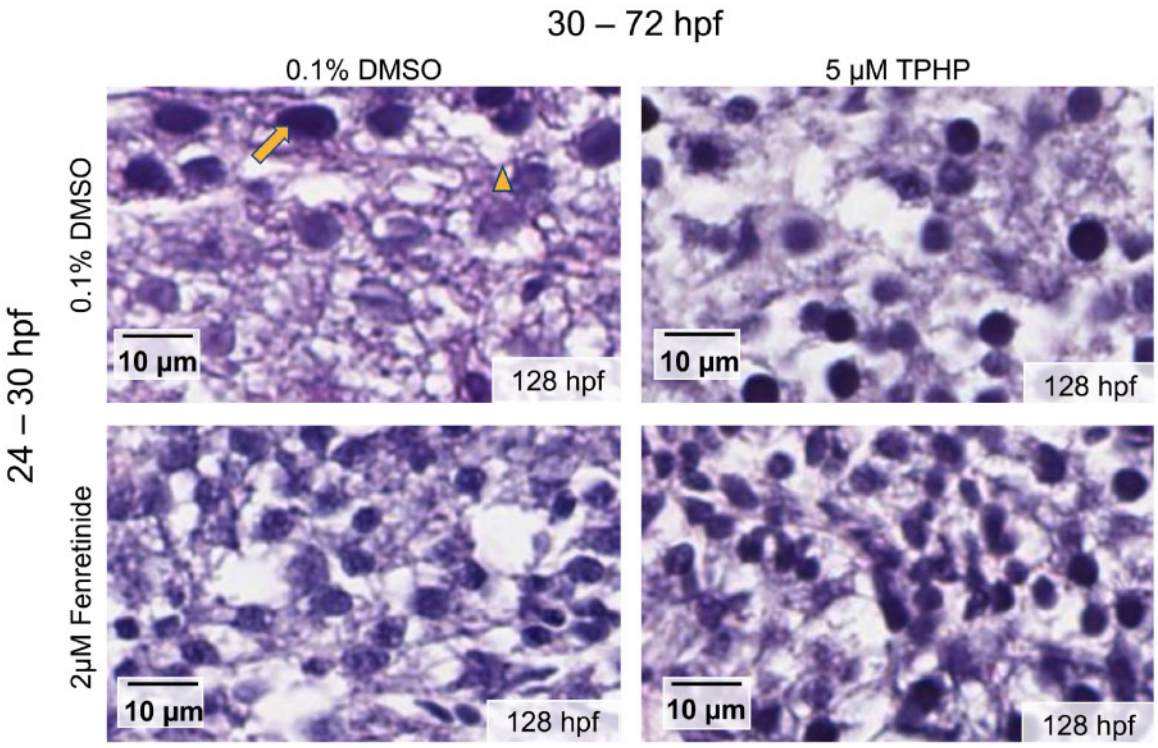

Figure 6. Representative histologic liver sections from 128-hpf embryos pretreated with vehicle (0.1% DMSO) or 2 μM fenretinide (Fen) from 24 to 30 hpf, treated with vehicle (0.1% DMSO) or 5 μM TPHP from 30 to 72 hpf, and then reared in clean system water until 128 hpf. Nuclei are stained with hematoxylin (arrow), proteins are stained with eosin, and empty spaces denote vacuolization (arrowhead) within the embryonic liver.

McGee *et al.*, 2013; Mitchell *et al.*, 2018), little is known about the target and mechanism of TPHP-induced cardiotoxicity during early development. Although cardiac looping occurs between 36 and 48 hpf (Bakkers, 2011), we found that initiation of TPHP exposure at 24 hpf did not result in cardiotoxicity before (30 hpf) or immediately after (48 hpf) cardiac looping, suggesting that TPHP-induced cardiotoxicity (detected at 72 hpf) occurs between 48 and 72 hpf. However, IPA's toxicity analysis revealed that transcripts associated with cardiotoxicity, hepatotoxicity, and nephrotoxicity were significantly affected by TPHP at 30 and 48 hpf, suggesting that effects on the transcriptome occurred in the absence of detectable effects on cardiac development.

Interestingly, although fenretinide (a pan-RAR agonist) blocked TPHP-induced pericardial edema, pretreatment with fenretinide did not block TPHP-induced effects on cardiotoxicity-related pathways, a finding consistent with our recent study demonstrating that fenretinide does not mitigate TPHP-induced effects on the distance between the sinus venosus and bulbus arteriosus (SV-BA) (Mitchell *et al.*, 2019). Fenretinide is a synthetic retinoid and analog of retinol (vitamin A) with known anti-inflammatory properties (Kanagaratham *et al.*, 2014). In mice, fenretinide decreases and increases the concentration of arachidonic acid (an initiator of inflammation) and docosahexaenoic acid (anti-inflammatory compound) (López-Vales *et al.*, 2010), respectively, resulting in a net decrease in inflammation and edema formation. As retinoic acid blocks edema formation within embryonic zebrafish following alcohol and paclobutrazol exposure (Marrs *et al.*, 2010; Wang *et al.*, 2017), fenretinide may have blocked TPHP-induced pericardial edema formation from 48 to 72 hpf by decreasing inflammation and/or fluid accumulation. Interestingly, based on biological processes identified by DAVID, ion transport was significantly altered after exposure to 10 μM TPHP—a biological process that was mitigated by pretreatment with 2 μM fenretinide. These data suggest that fenretinide may play a role in blocking TPHP-induced effects on ion transport and, as a result, edema formation.

TPHP induces cytotoxicity within hepatocytes derived from chicken embryos (Su *et al.*, 2014), and increases levels of reactive oxygen species in HepG2 cells (An *et al.*, 2018). Moreover, the rate of TPHP metabolism within human hepatocytes is slower compared to certain organophosphate flame retardants (eg, tris(2-butoxyethyl) phosphate), resulting in the potential for bioaccumulation and persistent toxicity within the liver (Van den Eede *et al.*, 2016). Within this study, IPA revealed that the majority of transcripts significantly affected by TPHP at 30 and 48 hpf were associated with hepatotoxicity pathways. Indeed, exposure to TPHP from 30 to 72 hpf resulted in an increase in liver area at 128 hpf. This effect occurred in the absence of detectable histologic changes (eg, necrosis, fatty liver, and inflammation) within the liver, suggesting that enlargement of the liver was not due to hepatocellular hypertrophy, hyperplasia, lipid accumulation, nor inflammation. In addition, TPHP-induced liver enlargement was blocked by pretreatment with fenretinide, suggesting that, similar to pericardial edema, fenretinide may block fluid accumulation within the liver.

Prior studies have shown that TPHP disrupts hepatic carbohydrate and lipid metabolism in adult zebrafish and mice (Du *et al.*, 2016; Wang *et al.*, 2019a), an effect that may be driven by activation of peroxisome proliferator-activated receptor γ (PPARγ) (Pillai *et al.*, 2014). Using Oil Red O staining, we found that TPHP exposure resulted in a concentration-dependent decrease in neutral lipids within the embryo (particularly within the head and trunk), an effect that was not blocked by

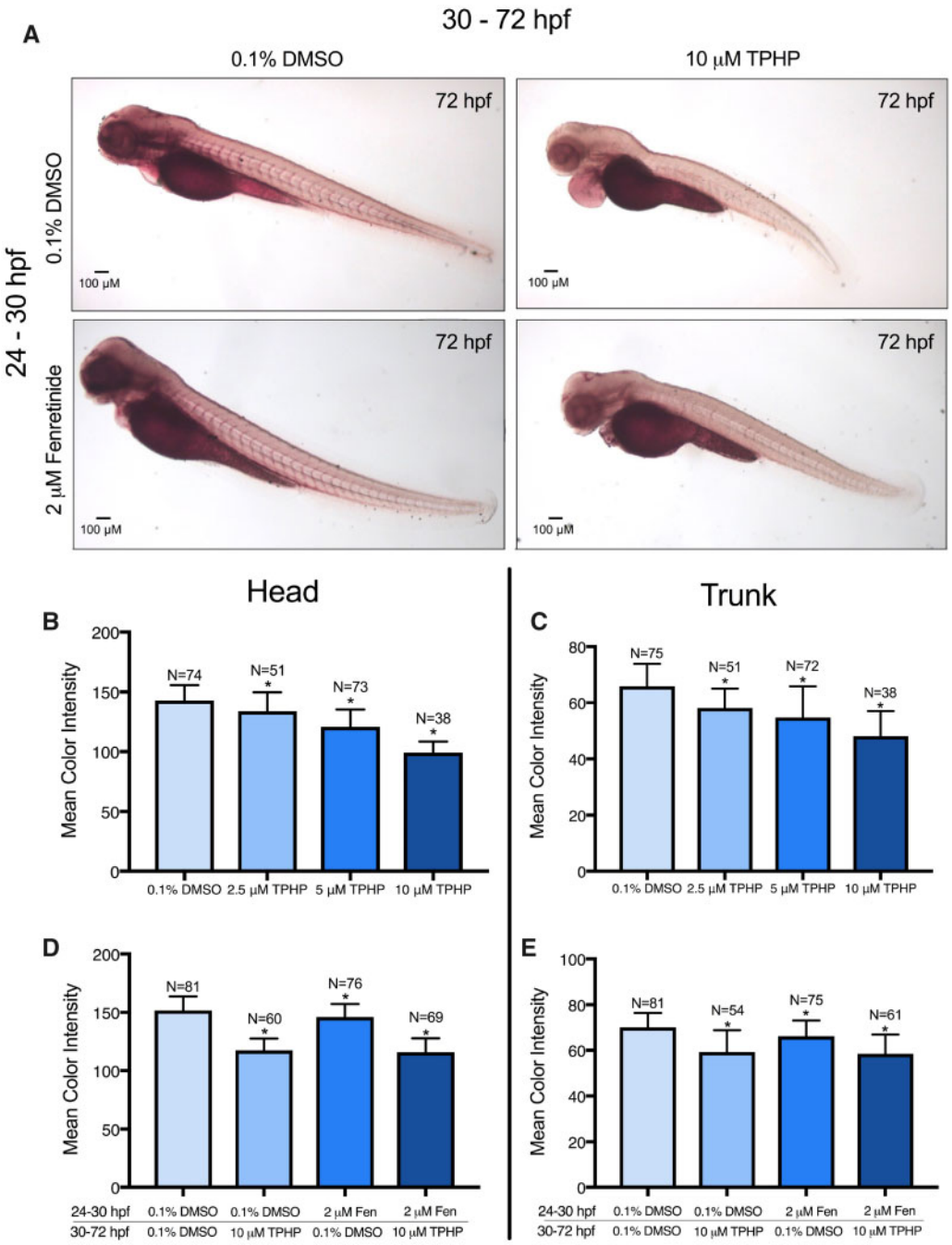

Figure 7. Oil Red O-stained representative images (A), mean color intensity (± standard deviation) of the head (B, D), and trunk (C, E) of 72-hpf embryos treated with either (1) vehicle (0.1% DMSO) or TPHP (triphenyl phosphate) (2.5, 5, or 10 μM) from 24 to 72 hpf or (2) pretreated with vehicle (0.1% DMSO) or 2 μM fenretinide (Fen) from 24 to 30 hpf and then treated with vehicle (0.1% DMSO) or 10 μM TPHP from 30 to 72 hpf. Asterisk (*) denotes $p < .05$.

pretreatment with fenretinide. Similarly, untargeted metabolomics revealed that TPHP resulted in a significant decrease in the total abundance of lipid-specific metabolites at 48 and 72 hpf. Within zebrafish, previous studies have demonstrated that a decrease in yolk sac-associated lipids from 48 to 72 hpf is accompanied by an increase in body-associated lipids (Fraher *et al.*, 2015). Therefore, TPHP may have an impact on the abundance, movement, and/or utilization of lipids from the yolk sac to the body from 48 to 72 hpf.

Among all of the metabolites quantified, betaine was the most significantly affected metabolite following TPHP exposure. In mice and humans, betaine plays an important role in liver and kidney function. Human patients with nonalcoholic liver diseases have significantly decreased hepatic betaine concentrations, suggesting that decreased betaine levels are associated with liver toxicity (Sookoian *et al.*, 2017). Within kidneys, betaine acts as an osmoprotectant to ensure that osmolarity is balanced to allow water reabsorption (Kempson *et al.*, 2013). Osmoprotectants raise the osmotic pressure in the cytoplasm by stabilizing enzyme and protein structures in order to maintain the structure of membranes when exposed to stress (McNeil *et al.*, 1999). Within our study, decreased betaine

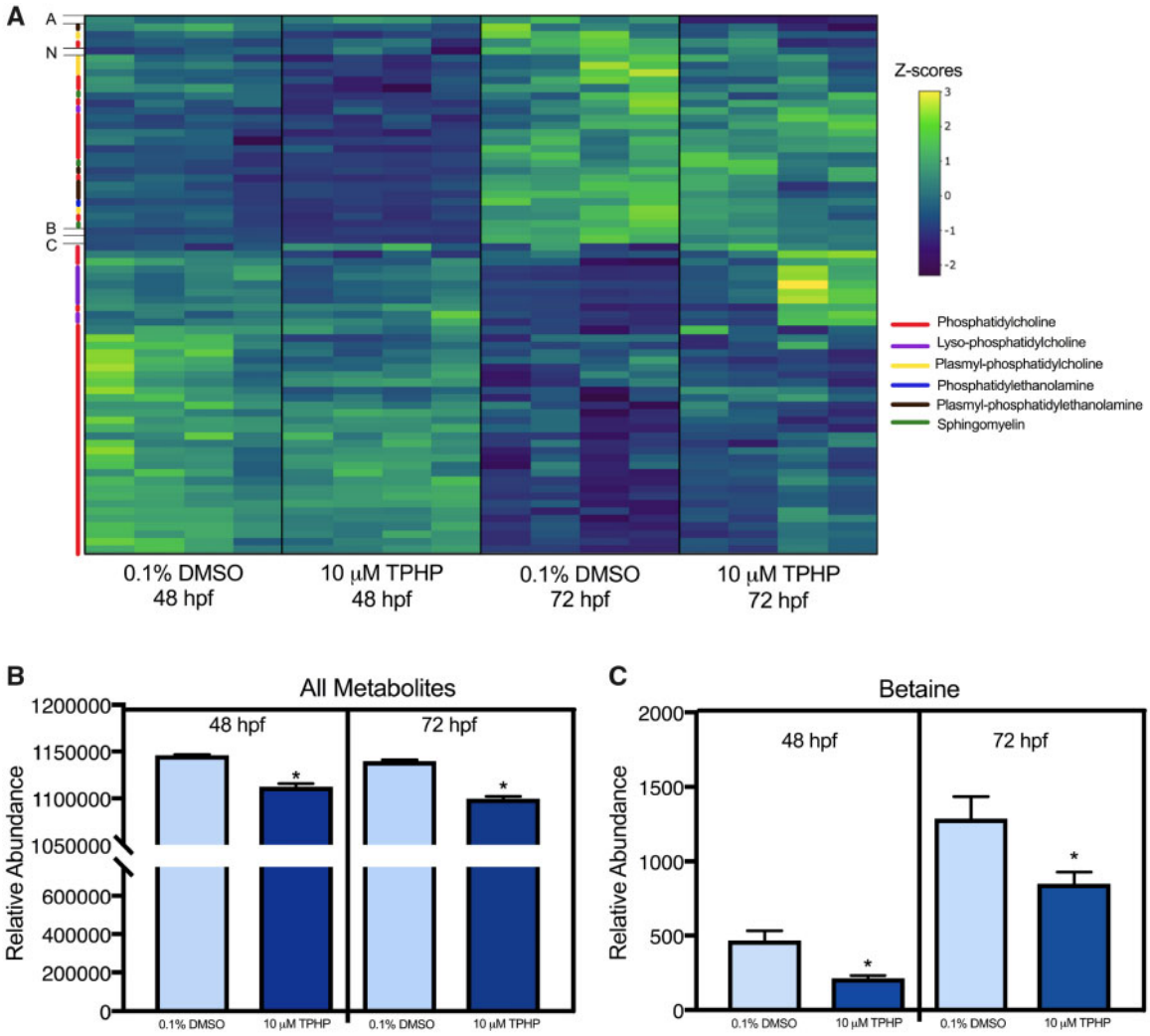

Figure 8. Untargeted metabolomics analysis (A) of 48- and 72-hpf embryos treated with either vehicle (0.1% DMSO) or 10 μM TPHP (triphenyl phosphate) from 30 to 48 hpf or 30 to 72 hpf, respectively. Data shown within the heat map are z-scored. Each column represents an individual biological replicate, each row represents an individual metabolite, and each color on the y-axis represents a different metabolite class represented within the legend to the right. Acylcarnitine 22:6 (A), N-acetylhistidine (N), betaine (B), and cholesterol/lathosterol (C) did not fall within any of the broader metabolite classes. Relative abundance (± standard deviation) of all metabolites (B) and betaine (C) within 48- and 72-hpf embryos treated with either vehicle (0.1% DMSO) or 10 μM TPHP from 30 to 48 hpf or 30 to 72 hpf, respectively.

concentrations following TPHP exposure may have precluded adaptation to osmotic stress, leading to disruption of osmotic balance and fluid accumulation throughout the entire embryo. As liver enlargement did not appear to be a result of hepatocellular hypertrophy, it is possible that an increase in liver area was due to accumulation of fluid within or surrounding the liver. Indeed, our recent study demonstrated that coexposure to TPHP and mannitol (an osmoprotectant) resulted in a significant decrease in pericardial edema and SV-BA length relative to TPHP-alone (Mitchell *et al.*, 2019), suggesting that the presence of an osmoprotectant in the surrounding water mitigates TPHP-induced fluid accumulation within zebrafish embryos.

In summary, our data collectively suggest that, in addition to cardiotoxicity, TPHP adversely affects hepatotoxicity-related pathways, liver morphology, neutral lipid abundance, and metabolite abundance within developing zebrafish embryos. Moreover, our data suggest that TPHP decreases baseline betaine concentrations, leading to potential direct effects on osmoregulation and indirect effects on organ development. However, additional research is needed to (1) determine if the addition of excess betaine mitigates TPHP-induced effects on the developing embryo and (2) determine whether PPARγ (a known target for TPHP) is required for TPHP-induced effects on osmoregulation.

SUPPLEMENTARY DATA

Supplementary data are available at *Toxicological Sciences* online.

DECLARATION OF CONFLICTING INTERESTS

The authors declared no potential conflicts of interest with respect to the research, authorship, and/or publication of this article.

FUNDING

This work was supported by a UCR Graduate Division Fellowship to A.R. and NRSA T32 Training Program

(T32ES018827 to C.A.M.), as well as a National Institutes of Health grant (R01ES027576); and USDA National Institute of Food and Agriculture Hatch Project (1009609 to D.C.V).

REFERENCES

An, J., Zheng, K., Zhong, Y., Yu, Z., Shang, Y., An, J., and Desk, S. (2018). Triphenyl phosphate (TPP) and tris (2-chloroisopropyl) phosphate (TCPP) induced apoptosis and cell cycle arrest in HepG2 cells. *SDRP J. Earth Sci. Environ. Stud.* **4**, 490–501.

Bakkers, J. (2011). Zebrafish as a model to study cardiac development and human cardiac disease. *Cardiovasc. Res.* **91**, 279–288.

Begemann, G., Marx, M., Mebus, K., Meyer, A., and Bastmeyer, M. (2004). Beyond the neckless phenotype: Influence of reduced retinoic acid signaling on motor neuron development in the zebrafish hindbrain. *Dev. Biol.* **271**, 119–129.

Broeckling, C. D., Afsar, F. A., Neumann, S., Ben-Hur, A., and Prenni, J. E. (2014). RAMClust: A novel feature clustering method enables spectral-matching-based annotation for metabolomics data. *Anal. Chem.* **86**, 6812–6817.

Ding, J., Xu, Z., Huang, W., Feng, L., and Yang, F. (2016). Organophosphate ester flame retardants and plasticizers in human placenta in eastern China. *Sci. Total Environ.* **554–555**, 211–217.

Du, Z., Zhang, Y., Wang, G., Peng, J., Wang, Z., and Gao, S. (2016). TPHP exposure disturbs carbohydrate metabolism, lipid metabolism, and the DNA damage repair system in zebrafish liver. *Sci. Rep.* **6**, 21827.

Dunn, W. B., Broadhurst, D., Begley, P., Zelena, E., Francis-McIntyre, S., Anderson, N., Brown, M., Knowles, J. D., Halsall, A., Haselden, J. N., *et al.* (2011). Procedures for large-scale metabolic profiling of serum and plasma using gas chromatography and liquid chromatography coupled to mass spectrometry. *Nat. Protoc.* **6**, 1060–1083.

Fraher, D., Ellis, M. K., Morrison, S., McGee, S. L., Ward, A. C., Walder, K., and Gibert, Y. (2015). Lipid abundance in zebrafish embryos is regulated by complementary actions of the endocannabinoid system and retinoic acid pathway. *Endocrinology* **156**, 3596–3609.

Harrad, S., Brommer, S., and Mueller, J. F. (2016). Concentrations of organophosphate flame retardants in dust from cars, homes, and offices: An international comparison. *Emerg. Contam.* **2**, 66–72.

He, C., Toms, L.-M. L., Thai, P., Van den Eede, N., Wang, X., Li, Y., Baduel, C., Harden, F. A., Heffernan, A. L., Hobson, P., *et al.* (2018). Urinary metabolites of organophosphate esters: Concentrations and age trends in Australian children. *Environ. Int.* **111**, 124–130.

Hong, X., Chen, R., Hou, R., Yuan, L., and Zha, J. (2018). Triphenyl phosphate (TPHP)-induced neurotoxicity in adult male Chinese rare minnows (*Gobiocypris rarus*). *Environ. Sci. Technol.* **52**, 11895–11903.

Isales, G. M., Hipszer, R. A., Raftery, T. D., Chen, A., Stapleton, H. M., and Volz, D. C. (2015). Triphenyl phosphate-induced developmental toxicity in zebrafish: Potential role of the retinoic acid receptor. *Aquat. Toxicol.* **161**, 221–230.

Jarema, K. A., Hunter, D. L., Shaffer, R. M., Behl, M., and Padilla, S. (2015). Acute and developmental behavioral effects of flame retardants and related chemicals in zebrafish. *Neurotoxicol. Teratol.* **52**, 194–209.

Kanagaratham, C., Kalivodová, A., Najdekr, L., Friedecký, D., Adam, T., Hajduch, M., De Sanctis, J. B., and Radzioch, D. (2014). Fenretinide prevents inflammation and airway hyperresponsiveness in a mouse model of allergic asthma. *Am. J. Respir. Cell Mol. Biol.* **51**, 783–792.

Kempson, S. A., Vovor-Dassu, K., and Day, C. (2013). Betaine transport in kidney and liver: Use of betaine in liver injury. *Cell. Physiol. Biochem.* **32**, 32–40.

Khairy, M. A., and Lohmann, R. (2019). Organophosphate flame retardants in the indoor and outdoor dust and gas-phase of Alexandria, Egypt. *Chemosphere* **220**, 275–285.

Kim, J.-W., Isobe, T., Muto, M., Tue, N. M., Katsura, K., Malarvannan, G., Sudaryanto, A., Chang, K.-H., Prudente, M., Viet, P. H., *et al.* (2014). Organophosphorus flame retardants (PFRs) in human breast milk from several Asian countries. *Chemosphere* **116**, 91–97.

Kim, S., Jung, J., Lee, I., Jung, D., Youn, H., and Choi, K. (2015). Thyroid disruption by triphenyl phosphate, an organophosphate flame retardant, in zebrafish (*Danio rerio*) embryos/larvae, and in GH3 and FRTL-5 cell lines. *Aquat. Toxicol.* **160**, 188–196.

Li, Y., Wang, C., Zhao, F., Zhang, S., Chen, R., and Hu, J. (2018). Environmentally relevant concentrations of the organophosphorus flame retardant triphenyl phosphate impaired testicular development and reproductive behaviors in Japanese medaka (*Oryzias latipes*). *Environ. Sci. Technol. Lett.* **5**, 649–654.

Liu, X., Jung, D., Jo, A., Ji, K., Moon, H.-B., and Choi, K. (2016). Long-term exposure to triphenylphosphate alters hormone balance and HPG, HPI, and HPT gene expression in zebrafish (*Danio rerio*). *Environ. Toxicol. Chem.* **35**, 2288–2296.

López-Vales, R., Redensek, A., Skinner, T. A. A., Rathore, K. I., Ghasemlou, N., Wojewodka, G., DeSanctis, J., Radzioch, D., and David, S. (2010). Fenretinide promotes functional recovery and tissue protection after spinal cord contusion injury in mice. *J. Neurosci.* **30**, 3220–3226.

Marrs, J. A., Clendenon, S. G., Ratcliffe, D. R., Fielding, S. M., Liu, Q., and Bosron, W. F. (2010). Zebrafish fetal alcohol syndrome model: Effects of ethanol are rescued by retinoic acid supplement. *Alcohol* **44**, 707–715.

McGee, S. P., Konstantinov, A., Stapleton, H. M., and Volz, D. C. (2013). Aryl phosphate esters within a major pentaBDE replacement product induce cardiotoxicity in developing zebrafish embryos: Potential role of the aryl hydrocarbon receptor. *Toxicol. Sci.* **133**, 144–156.

McNeil, S. D., Nuccio, M. L., and Hanson, A. D. (1999). Betaines and related osmoprotectants. Targets for metabolic engineering of stress resistance. *Plant Physiol.* **120**, 945–949.

Mitchell, C. A., Dasgupta, S., Zhang, S., Stapleton, H. M., and Volz, D. C. (2018). Disruption of nuclear receptor signaling alters triphenyl phosphate-induced cardiotoxicity in zebrafish embryos. *Toxicol. Sci.* **163**, 307–318.

Mitchell, C. A., Reddam, A., Dasgupta, S., Zhang, S., Stapleton, H. M., and Volz, D. C. (2019). Diphenyl phosphate-induced toxicity during embryonic development. *Environ. Sci. Technol.* **53**, 3908–3916.

Morris, P. J., Medina-Cleghorn, D., Heslin, A., King, S. M., Orr, J., Mulvihill, M. M., Krauss, R. M., and Nomura, D. K. (2014). Organophosphorus flame retardants inhibit specific liver carboxylesterases and cause serum hypertriglyceridemia. *ACS Chem. Biol.* **9**, 1097–1103.

Ospina, M., Jayatilaka, N. K., Wong, L.-Y., Restrepo, P., and Calafat, A. M. (2018). Exposure to organophosphate flame retardant chemicals in the U.S. general population: Data from the 2013–2014 National Health and Nutrition Examination Survey. *Environ. Int.* **110**, 32–41.

Passeri, M. J., Cinaroglu, A., Gao, C., and Sadler, K. C. (2009). Hepatic steatosis in response to acute alcohol exposure in zebrafish requires sterol regulatory element binding protein activation. *Hepatology* **49**, 443–452.

Pillai, H. K., Fang, M., Beglov, D., Kozakov, D., Vajda, S., Stapleton, H. M., Webster, T. F., and Schlezinger, J. J. (2014). Ligand binding and activation of PPARγ by Firemaster® 550: Effects on adipogenesis and osteogenesis in vitro. *Environ. Health Perspect.* **122**, 1225–1232.

Rantakokko, P., Kumar, E., Braber, J., Huang, T., Kiviranta, H., Cequier, E., and Thomsen, C. (2019). Concentrations of brominated and phosphorous flame retardants in Finnish house dust and insights into children's exposure. *Chemosphere* **223**, 99–107.

Samarut, E., Fraher, D., Laudet, V., and Gibert, Y. (2015). ZebRA: An overview of retinoic acid signaling during zebrafish development. *Biochim. Biophys. Acta* **1849**, 73–83.

Schymanski, E. L., Jeon, J., Gulde, R., Fenner, K., Ruff, M., Singer, H. P., and Hollender, J. (2014). Identifying small molecules via high resolution mass spectrometry: Communicating confidence. *Environ. Sci. Technol.* **24**, 2097–2098.

Shi, Q., Wang, M., Shi, F., Yang, L., Guo, Y., Feng, C., Liu, J., and Zhou, B. (2018). Developmental neurotoxicity of triphenyl phosphate in zebrafish larvae. *Aquat. Toxicol.* **203**, 80–87.

Shi, Q., Wang, Z., Chen, L., Fu, J., Han, J., Hu, B., and Zhou, B. (2019). Optical toxicity of triphenyl phosphate in zebrafish larvae. *Aquat. Toxicol.* **210**, 139–147.

Sookoian, S., Puri, P., Castaño, G. O., Scian, R., Mirshahi, F., Sanyal, A. J., and Pirola, C. J. (2017). Nonalcoholic steatohepatitis is associated with a state of betaine-insufficiency. *Liver Int.* **37**, 611–619.

Stafford, D., and Prince, V. E. (2002). Retinoic acid signaling is required for a critical early step in zebrafish pancreatic development. *Curr. Biol.* **12**, 1215–1220.

Stainier, D. Y. R., and Fishman, M. C. (1992). Patterning the zebrafish heart tube: Acquisition of anteroposterior polarity. *Dev. Biol.* **153**, 91–101.

Stapleton, H. M., Klosterhaus, S., Eagle, S., Fuh, J., Meeker, J. D., Blum, A., and Webster, T. F. (2009). Detection of organophosphate flame retardants in furniture foam and US house dust. *Environ. Sci. Technol.* **43**, 7490–7495.

Su, G., Crump, D., Letcher, R. J., and Kennedy, S. W. (2014). Rapid in vitro metabolism of the flame retardant triphenyl phosphate and effects on cytotoxicity and mRNA expression in chicken embryonic hepatocytes. *Environ. Sci. Technol.* **48**, 13511–13519.

Sumner, L. W., Amberg, A., Barrett, D., Beale, M. H., Beger, R., Daykin, C. A., Fan, T. W., Fiehn, O., Goodacre, R., Griffin, J. L., *et al.* (2007). Proposed minimum reporting standards for chemical analysis Chemical Analysis Working Group (CAWG) Metabolomics Standards Initiative (MSI). *Metabolomics* **3**, 211–221.

Sun, Y., Gong, X., Lin, W., Liu, Y., Wang, Y., Wu, M., Kannan, K., and Ma, J. (2018). Metabolites of organophosphate ester flame retardants in urine from Shanghai, China. *Environ. Res.* **164**, 507–515.

Sun, Y., Liu, L.-Y., Sverko, E., Li, Y.-F., Li, H.-L., Huo, C.-Y., Ma, W.-L., Song, W., and Zhang, Z.-F. (2019). Organophosphate flame retardants in college dormitory dust of northern Chinese cities: Occurrence, human exposure and risk assessment. *Sci. Total Environ.* **665**, 731–738.

Van den Eede, N., de Meester, I., Maho, W., Neels, H., and Covaci, A. (2016). Biotransformation of three phosphate flame retardants and plasticizers in primary human hepatocytes: Untargeted metabolite screening and quantitative assessment. *J. Appl. Toxicol.* **36**, 1401–1408.

van der Veen, I., and de Boer, J. (2012). Phosphorus flame retardants: Properties, production, environmental occurrence, toxicity and analysis. *Chemosphere* **88**, 1119–1153.

Wang, D., Yan, S., Yan, J., Teng, M., Meng, Z., Li, R., Zhou, Z., and Zhu, W. (2019). Effects of triphenyl phosphate exposure during fetal development on obesity and metabolic dysfunctions in adult mice: Impaired lipid metabolism and intestinal dysbiosis. *Environ. Pollut.* **246**, 630–638.

Wang, L., Huang, X., Laserna, A. K. C., and Li, S. F. Y. (2018). Untargeted metabolomics reveals transformation pathways and metabolic response of the earthworm *Perionyx excavatus* after exposure to triphenyl phosphate. *Sci. Rep.* **8**, 16440.

Wang, L., Huang, X., Lim, D. J., Laserna, A. K. C., and Li, S. F. Y. (2019). Uptake and toxic effects of triphenyl phosphate on freshwater microalgae *Chlorella vulgaris* and *Scenedesmus obliquus*: Insights from untargeted metabolomics. *Sci. Total Environ.* **650**, 1239–1249.

Wang, W.-D., Hsu, H.-J., Li, Y.-F., and Wu, C.-Y. (2017). Retinoic acid protects and rescues the development of zebrafish embryonic retinal photoreceptor cells from exposure to paclobutrazol. *Int. J. Mol. Sci.* **18**, 130.

Wingert, R. A., Selleck, R., Yu, J., Song, H.-D., Chen, Z., Song, A., Zhou, Y., Thisse, B., Thisse, C., McMahon, A. P., *et al.* (2007). The cdx genes and retinoic acid control the positioning and segmentation of the zebrafish pronephros. *PLoS Genet.* **3**, e189.

Yozzo, K. L., Isales, G. M., Raftery, T. D., and Volz, D. C. (2013). High-content screening assay for identification of chemicals impacting cardiovascular function in zebrafish embryos. *Environ. Sci. Technol.* **47**, 11302–11310.

Yutzey, K. E., and Bader, D. (1995). Diversification of cardiomyogenic cell lineages during early heart development. *Circ. Res.* **77**, 216–219.